Lawrence Berkeley National Laboratory
Recent Work

Title
SHAKE-OFF ON INNER-SHELL RESONANCES OF Ar, Kr, AND Xe

Permalink
https://escholarship.org/uc/item/5z48x7br

Author
Heimann, P.A.

Publication Date
1986-12-01

Lawrence Berkeley Laboratory
UNIVERSITY OF CALIFORNIA

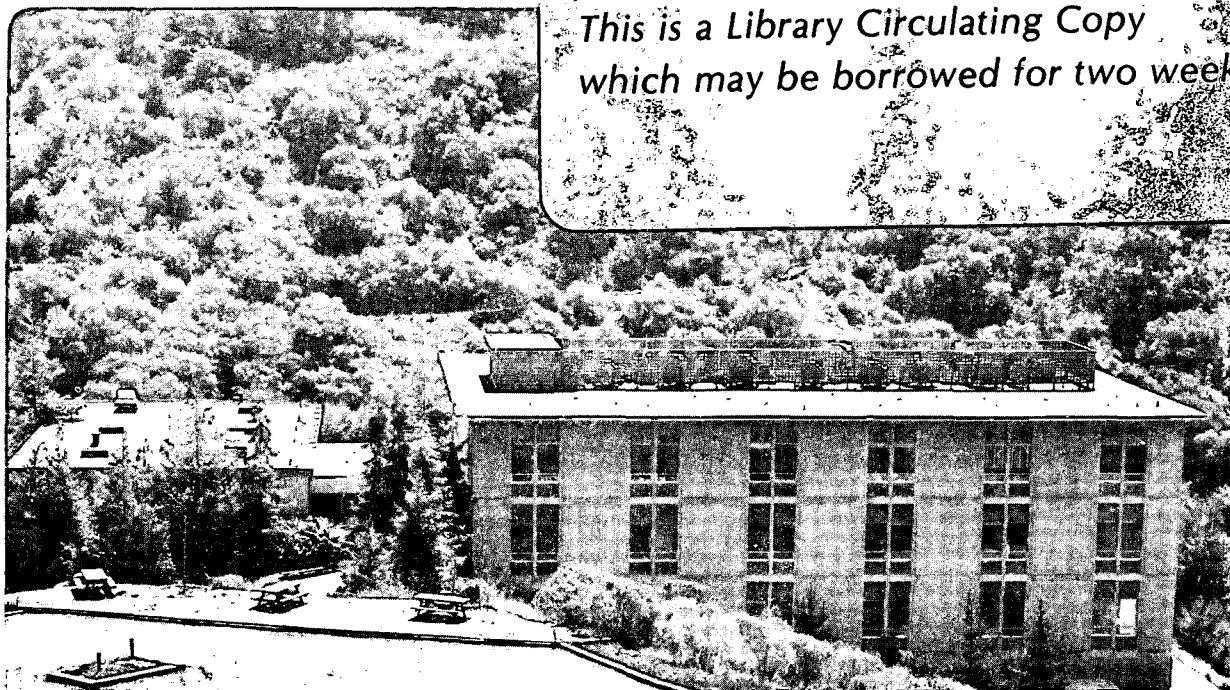## Materials & Molecular Research Division

SHAKE-OFF ON INNER-SHELL
RESONANCES OF Ar, Kr, and Xe

P.A. Heimann, D.W. Lindle, T.A. Ferrett,
S.H. Liu, L.J. Medhurst, M.N. Piancastelli,
D.A. Shirley, U. Becker, H.G. Kerkhoff,
B. Langer, D. Szostak, and R. Wehlitz

December 1986

DISCLAIMER

LBL-22412

Shake-off on inner-shell resonances of Ar, Kr, and Xe

P A Heimann,[1][*] D W Lindle,[1][†] T A Ferrett,[1][¶] S H Liu,[1] L J Medhurst,[1] M N Piancastelli,[1][**] D A Shirley,[1] U Becker,[2] H G Kerkhoff,[2] B Langer,[2] D Szostak,[2] and R Wehlitz[2]

[1]Materials and Molecular Research Division, Lawrence Berkeley Laboratory, and Department of Chemistry, University of California, Berkeley, California 94720, USA

[2]Technische Universität Berlin, Institut für Strahlungs- and Kernphysik, Sekr, PN 3-2, Hardenbergstrasse 36, D-1000 Berlin 12, Federal Republic of Germany

Abstract.

Synchrotron radiation was used to excite an inner-shell electron into a Rydberg orbital at the Ar 2p → ns, nd, Kr 3d → np, and Xe 4d → np resonances. The resonant decay into shake-off channels was studied by three different electron measurements. First, threshold electron scans were obtained over the resonances and thresholds. On the first resonance for each atom, photoelectron spectra were collected. The intensity distribution of low kinetic energy electrons was also determined for a few resonances. Finally, a shake calculation was carried out to compare with the experimental shake-off probabilities. Shake-off is observed to be a strong decay channel for these resonances.

[*]Present address: Technische Universität München, D-8046 Garching b, München, Federal Republic of Germany.

[†]Present address: National Bureau of Standards, Quantum Metrology Group, Physics A141, Gaithersburg, MD 20899.

¶Present address: National Bureau of Standards, Physics A251,

Gaithersburg, MD 20899.

**Permanent address: II University of Rome, 00173 Rome, Italy.

1. Introduction

A threshold marks the photon energy at which electron ionization in a particular subshell becomes energetically allowed. For inner shells, the step-like onset of photoionization is complicated by two phenomena: discrete resonances and post-collision interaction (PCI). We discuss both briefly as background for the present work on threshold phenomena in rare gases.

At certain energies below threshold, an inner-shell electron may be excited into an unoccupied Rydberg orbital. In krypton, for example, two strong series of resonances have been observed: $3d_{5/2} \rightarrow 5p, 6p, \ldots$ and $3d_{3/2} \rightarrow 5p, 6p, \ldots$ (Codling and Madden 1964). Transitions to nf orbitals are quite weak because of the large barrier in the effective potential for f electrons (Fano and Cooper 1968). Resonances similarly occur in argon below the 2p thresholds and in xenon approaching the 4d thresholds.

A number of recent experiments have studied different aspects of the excitation and decay of a particular set of resonances - Ar 2p → ns, nd, Kr 3d → np and Xe 4d → np - which have been studied together because of their similarity as inner-shell resonances. Using electron impact, King et al (1977, 1985) measured energy-loss spectra, equivalent to photoabsorption scans. Their high-resolution experiment provides precise energies for the resonances and thresholds. Relative values of the oscillator strength f were determined and found to vary approximately with the separation of the resonance energy levels dE_n/dn. The decrease in intensity along a Rydberg series results mainly from the overall expansion of the Rydberg orbital (Fano and Cooper 1965). For a

given spin-orbit pair of resonances, e.g. Kr $3d_{5/2} \rightarrow np$ and $3d_{3/2} \rightarrow np$, the measured ratios of oscillator strengths were very close to statistical, suggesting that relativistic effects have little influence on the transition strengths of these resonances.

Combining synchrotron radiation and mass spectrometry, Hayaishi et al (1984) examined the cross sections σ for the formation of singly, doubly, and triply charged ions. For the argon 2p → ns, nd excitations, Ar^+ was found to be the most frequent product of resonant decay. By contrast, in both krypton and xenon the doubly charged ion is the dominant product at the d → np resonances. The Kr and Xe results were unexpected because the spectator model, in which the Rydberg electron remains in an outer orbital while the core undergoes an Auger-like decay, yields a singly-charged ion. Secondly, the linewidths (and consequently the lifetimes) of the Kr and Xe resonances were found to be essentially independent of the principal quantum number n of the Rydberg electron, which suggests that autoionization to the valence s^{-1} and p^{-1} final states rarely occurs. The Rydberg electron could participate in the resonant decay in some other way, such as being excited (shake-up) or ionized (shake-off). For the most important pathway to doubly-charged ions, Hayaishi et al (1984) proposed a two-step process, such as Kr $3d_{5/2}^{-1}5p \rightarrow Kr^+ \; 4s^{-1}4p^{-1}5p \rightarrow Kr^{+2} \; 4p^{-2}$, rather than a shake-off process.

Electron spectra at the Kr and Xe resonances have been investigated extensively. For both Kr (Lindle et al 1986) and Xe (Southworth et al 1983, Becker et al 1986), the observed variations in valence σ_{ns} and σ_{np} caused by autoionization were small, < 15 %. The electron spectra agree

with the expectations of the spectator model with two important

exceptions. First, shake-up of the Rydberg electron during Auger-like

decay contributes additional peaks, e.g. Kr $3d^{-1}5p \rightarrow Kr^{+} 4p^{-2}6p$ (Schmidt

et al 1981, Aksela et al 1986a, b, Lindle et al 1986). Secondly, on the

Xe $4d \rightarrow np$ resonances, Becker et al (1986) qualitatively observed a

large continuous background caused by shake-off processes, e.g. Xe

$4d^{-1}6p \rightarrow Xe^{2+} 5p^{-2}$. At the Xe $4d_{5/2} \rightarrow 6p$ resonance, Becker et al (1984)

observed shake-off to contribute 44 % of the total resonant intensity,

without the nonresonant σ_{sat}, σ_{5s} and σ_{5p}.

We now address post-collision interaction (PCI) effects. At photon

energies above but still close to threshold, photoemission and

"subsequent" Auger decay cannot be separated into two independent steps.

Niehaus (1977) developed a semi-classical model to explain PCI.

Initially, the slow photoelectron moves in the Coulomb field of the

singly charged ion A^{+}. As Auger emission occurs, the photoelectron

finds itself on the more strongly attractive potential curve of the

doubly charged ion A^{+2}. Recently, the Niehaus theory has been extended

by Russek and Mehlhorn (1986) to include the time for the Auger electron

to "overtake" the photoelectron. Predictions of the new model have been

confirmed by a measurement of Xe $N_{5}O_{23}O_{23}$ $^{1}S_{0}$ Auger electrons by Borst

and Schmidt (1986). PCI also causes the Ar^{+} yield to decrease slowly

above the $2p_{1/2}$ threshold as the probability for capture of the

photoelectron decreases (Hayaishi et al 1984). At the Kr 3d and Xe 4d

thresholds, however, Hayaishi et al (1984) surprisingly found no

evidence for PCI in the Kr and Xe ion cross sections.

Wight and Van der Wiel (1977) reported a low-resolution (1 eV) threshold scan of Xe over the 4d region. In a threshold spectrum the ejected electrons with very low kinetic energies are collected while varying the photon energy (or equivalently the energy loss of the impact electron). The threshold electron intensity from Xe was enhanced at the below-threshold resonances because of shake-off transitions, e.g. Xe $4d^{-1}nl \rightarrow Xe^{2+} 5p^{-2}$. Wight and Van der Wiel also observed that the Xe 4d threshold peaks were distorted by PCI, having a lowered maximum and a tail extending to higher energy.

In this work, we have used high-resolution synchrotron radiation to take threshold electron scans over the Ar 2p, Kr 3d, and Xe 4d threshold regions. Our main purpose was to study quantitatively the shake-off transitions occuring on the below-threshold resonances. We also have determined the threshold lineshapes for comparison with the PCI theory. To measure the total intensity of shake-off electrons on the resonances, photoelectron spectra and intensity distributions of low kinetic energy electrons were obtained. Lastly, a shake calculation of the shake-off probability was carried out using Hartree-Fock (HF) wavefunctions.

Some experimental methods are described in Sec. 2. Sec. 3 is devoted to the intensities of threshold electrons on the below-threshold resonances and Sec. 4 to the threshold lineshape. Sec. 5 contains the discussion of the photoelectron spectra and the intensity distributions of low kinetic electrons. The results of the shake calculation are described in Sec. 6. Finally, the conclusions are presented in Sec. 7.

2. Experimental

This experiment was performed at the Stanford Synchrotron Radiation Laboratory (SSRL) using a grazing incidence "grasshopper" monochromator. Some work on Xe was carried out at the 5.6 m toroidal grating monochromator (TGM) at the Hamburger Synchrotronstrahlungslabor (HASYLAB). In the SSRL studies, two gratings were employed, with 600 and 1200 lines/mm. An Al filter was inserted to reduce the higher-order light of the 600 lines/mm grating. For the threshold electron scans, the monochromator resolution (FWHM) is estimated to be 0.35 eV for Ar and 0.04 eV for Kr and Xe. For the low kinetic energy distributions and photoelectron spectra which require higher flux, the monochromator bandwidth was broader: 1 eV for Ar and 0.2 eV for Kr and Xe.

The threshold scans and low kinetic energy distributions were obtained with a threshold electron analyzer similar to the one described in detail in an earlier paper (Heimann et al 1986). Briefly, photoelectrons are extracted by a weak electric field from the interaction region, which results in a very high transmission for zero and low kinetic energies. Following the principle of space focussing (Wiley and McLaren 1955), the electrons are energy-analyzed by their flight times between the interaction region and the detector. There are a few differences between the threshold electron analyzer used in the present work and the one described earlier (Heimann et al 1986). In this spectrometer the flight path is shorter (215 mm). The angle between the electric vector and the analyzer axis is fixed at 55°, the magic angle, which implies that the measured electron intensities are

independent of angular distribution effects. Lastly, during a photon-energy scan, an entire time spectrum is stored for each photon energy. Afterwards, in the data analysis of a single scan, different kinetic energies may be selected by choosing the appropriate energy (time) window. The threshold intensity represents the electron count rate inside a kinetic energy (time) window set to include energies from 0.0 to 0.05 eV. This electron signal is then divided by the photon flux monitored by a sodium salicylate scintillator and photomultiplier tube.

Low kinetic energy distributions of Kr were constructed by varying the kinetic energy window in 0.2 eV steps from 0 to 10 eV. For each of these energies, the intensity of the resonance was divided by that of the 3d photoelectron peaks. These ratios, which are independent of the analyzer transmission, are then multiplied by σ_{3d} to obtain the electron intensity distributions. Unfortunately, at these low kinetic energies σ_{3d} is not well known. We inferred σ_{3d} from the increased threshold electron signal above the 3d thresholds, caused by double-Auger transitions: $Kr^+ \ 3d^{-1} \rightarrow Kr^{3+} \ 4p^{-3}$. The double-Auger intensity was estimated down to 1.6 eV kinetic energy and then extrapolated to the average 3d threshold. From this analysis, σ_{3d} is observed to increase nearly linearly by 70 % from 0 to 10 eV kinetic energy. This result for σ_{3d} agrees better with the HF calculation of Manson and Kennedy (1972) than with the measurement of Carlson et al (1982). We estimate the combined statistical and calibration uncertainty to be 25 %.

In addition to the threshold scans and low kinetic energy distributions, photoelectron spectra were taken with our other time-of-flight electron spectrometers, where, as is more usual, electrons first

travel through a field free region before being accelerated, as in this case, or decelerated. These analyzers described by White et al (1979) have a slowly varying transmission function. The photoelectron spectra have been obtained in 2000 s both at 0° and 55° with respect to the light polarization vector. The spectra taken at the two angles gave the same results within error, which implies that β for shake-off is close to 0. Off-resonant spectra have been subtracted in order to account for the analyzer dark counts and the photoelectrons resulting from second-order light. Secondly, the spectra have been corrected for the analyzer transmission function as determined by calibration with Ne 2s and 2p photoelectron peaks. The analyzer resolution varies with kinetic energy as 0.04·E for the 0° analyzer and as 0.05·E for the 54° analyzer.

3. Threshold electron intensities, resonant shake-off

Figures 1, 2, and 3 display threshold scans over the Ar 2p, Kr 3d, and Xe 4d thresholds. Table 1 shows the relative oscillator strengths f from King et al (1977, 1985) and the relative threshold intensities obtained from fits of the scans shown in Figs. 1, 2, and 3. The values of f on the resonances were inferred from King et al's Eq. (5) and the reported df/dE and n^*.

The threshold scans contain the following features: a constant level at lower energies from the analyzer background and valence shake-off, e.g. $Kr + h\nu \rightarrow Kr^{2+} 4p^4 + 2e^-$, and a constant signal above the thresholds, which is higher as a result of double Auger events, e.g., $Kr^+ 3d^{-1} 4p^6 \rightarrow Kr^{3+} 4p^3 + 2e^-$. Strong, nearly Lorentzian peaks are observed at resonances below threshold from the shake-off decay of the

excited state, e.g. Kr $3d^{-1}5p \rightarrow Kr^{2+} 4p^4 + 2e^-$. These resonant shake-off transitions resemble the double Auger events above threshold. Finally, at the inner-shell thresholds, there are peaks due to near 0 eV kinetic energy photoelectrons, e.g. $Kr + h\nu \rightarrow Kr^+ 3d^{-1} + e^-$, which are broadened and shifted to higher photon energy $h\nu$ by the post-collision interaction (PCI) between the slow photoelectron and the faster Auger electron.

In considering the threshold intensity on the resonances, it should be kept in mind that many of the possible decay channels produce ejected electrons with high kinetic energy, such as the spectator Auger-like decay $Kr \, 3d^{-1}5p \rightarrow Kr^+ \, 4p^{-2}5p + e^-$. Even shake-off decay rarely produces an electron with low enough kinetic energy to be included in the threshold scan because, in general, tens of electron volts of energy are partitioned between two electrons. In contrast, at threshold, all of the inner-shell photoelectrons will have the correct low energy to contribute to the threshold intensity. The prominent appearance of the resonances is therefore quite remarkable.

To interpret intensities of resonances in the threshold scans, it is necessary to place the threshold intensities on some scale of oscillator strength. On a resonance, the threshold intensity I_{th} will depend first on the shake-off oscillator strength f_s. A second factor is the functional form of the continuous distribution of shake-off electrons df_s/dKE, since the threshold analyzer detects only a small part of this distribution near 0 eV kinetic energy. Including the analyzer collection efficiency $e(KE)$,

$$I_{th} = \int_0^{\Delta E} \frac{df_s}{dKE} e(KE)dKE \quad \sim \quad \frac{df_s}{dKE}\bigg|_0 e_{av} \, \Delta E, \tag{1}$$

where e_{av} is an average analyzer efficiency for the accepted electrons

with energies from 0 to ΔE. At a threshold the total oscillator

strength is collected:

$$I_{th} = \int_0^{\Delta E} \frac{df}{dh\nu} \ e(KE)dh\nu - \left.\frac{df}{dh\nu}\right|_{BE} e_{av} \ \Delta E. \qquad (2)$$

By dividing I_{th} at the threshold by the known df/dE, a constant $N =$

$e_{av}\Delta E$ is obtained, which also includes the arbitrary scaling constant of

the relative absorption and threshold measurements. Finally at each

resonance,

$$\frac{I_{th}}{Nf} - \left.\frac{1}{f}\frac{df_s}{dKE}\right|_0, \qquad (3)$$

which is the fraction of the resonance resulting in shake-off with an

electron at low kinetic energy. The resulting values are displayed in

the last column of Table 1.

In the preceding derivation, it was assumed that two electrons from

the same ionization event do not fall within the analyzer kinetic-energy

window and that the shake-off distribution is slowly varying over this

window. The narrow analyzer resolution (0.1 eV) implies that both these

approximations are reasonable. In analyzing the threshold electron

spectrum of N_2O, Baer et al (1979) carried out a similar analysis

comparing (threshold electron) / (ion) ratios at autoionizing resonances

and at threshold.

For all the Kr and Xe resonances in Table 1, we note first that the

threshold shake-off fractions are surprisingly large, which implies that

shake-off is an important decay path. Secondly, for all three atoms the

fractional yield of a resonance leading to low-energy electrons

increases with n. This n dependence suggests that in the shake-off

decay the Rydberg electron is usually ejected along with a valence

electron. For the higher-n resonances the Rydberg electron becomes less strongly bound, and the ejection of this electron should become more facile. In comparison, Kr and Xe ion-yield measurements (Hayaishi et al 1984, Eland et al 1986) showed the fractions of single and double ions varying slowly over the resonances, while the triple ion increases with n. In the case of Xe, Eland et al (1986) have proposed that Xe^{2+} results mainly from two step processes while Xe^{3+} is produced by direct shake-off. The ion-yield measurements imply that the cross section for shake-off decay increases with n. The variation of the threshold intensities with n can only suggest an n dependence for the total shake-off strength. The kinetic-energy distribution is another factor, which will be seen below to vary from one resonance to another.

Ar shows different behavior, having very low threshold intensities on the first two resonances and intensities similar to Kr and Xe on the unresolved higher resonances. The ion yields on the Ar resonances also differ from Kr and Xe (Hayaishi et al 1984). The Ar $2p^{-1}nl$ configurations decay mainly to singly charged ions. The fraction of double and triple ions that do result increases strongly with n. Apparently, shake-off is unusually weak for the lower resonances of Ar.

For a mechanism to contribute to the threshold electron intensity on resonance, at least two electrons must be ejected at once. The excess energy is shared, with a finite probability of either electron having very little kinetic energy. Consequently, the predominant pathways for creating threshold electrons should be single step decays from the neutral excited state to doubly- and triply-charged ion final states. Figure 4 shows three possible shake-off decay paths from the

$3d^{-1}5p$ resonant state of Kr in which: (1) two valence electrons are ejected, (2) the Rydberg electron is ejected along with a valence electron, and (3) the Rydberg electron and two valence electrons are ejected. For path (1), the same orbitals nl are involved as in double Auger above threshold, e.g. $Kr^+ 3d^{-1} \rightarrow Kr^{3+} 4p^{-3}$. The double Auger signal intensity, divided by the intensity of the threshold peaks, $Kr \rightarrow Kr^+ 3d^{-1}$, yields an Auger yield ratio R. The values of R determined from the data shown in Figs. 1-3 are $0.010(2)$ eV^{-1} (Ar), $0.028(9)$ eV^{-1} (Kr), and $0.15(2)$ eV^{-1} (Xe). These R values may provide an estimate for the contribution of the ejection of two valence electrons to the resonant threshold intensities, when compared with the values of $\frac{1}{f} \frac{df_s}{dKE}\bigg|_0$ given in column 6 of Table 1. For Xe, where σ_{4d} rises steeply from threshold, this double Auger intensity must be considered as an upper bound. Since the Rydberg electron does not change its orbital, the probability of ejecting two valence electrons should be nearly independent of n. In most of the cases in Table 1, this type of resonant shake-off seems to contribute a significant minority share of the threshold electron intensity.

The relative importance of the other kinds of shake-off are more difficult to evaluate. Shake-off to the triply-charged ion is expected to be important at threshold because it ejects three electrons sharing relatively little energy, e.g. Kr $3d_{5/2}^{-1}5p \rightarrow 4p^{-3} + 3e^-$, where the total available kinetic energy is 15.7 eV (Moore 1952).

The spin-orbit branching ratios for ionization at zero kinetic energy are determined from the intensities of the two threshold peaks: $2p_{3/2}/2p_{1/2} = 1.63(5)$ (Ar), $3d_{5/2}/3d_{3/2} = 1.6(1)$ (Kr), and $4d_{5/2}/4d_{3/2} =$

1.8(1) (Xe). In Ar and Xe, deviations are observed in opposite
directions from the statistical ratios of 2 and 1.5, respectively. In
general, it is expected that the branching ratio near threshold should
be greater than statistical because the $j=l+1/2$ orbital will be slightly
more diffuse and will have better overlap with the low-energy continuum
orbital (Walker and Waber 1974). Because of the delayed onset in the d
→ ϵf channel, the p wave should dominate at threshold for Kr and Xe
(Fano and Cooper 1968). The branching ratios of King et al (1977, 1985)
agree with our results for Ar and Kr, but disagree for Xe, where their
result is 1.3(2). Both Auger electron (Southworth et al 1983) and
photoelectron experiments (Yates et al 1985) have shown greater than
statistical values for Xe. Unfortunately, quantative comparison cannot
be made with those branching ratios, because they were determined with
both spin-orbit components at the same photon energy. Another Auger-
electron measurement (Aksela et al 1985) has shown the Kr $3d_{5/2}:3d_{3/2}$
ratio to be very close to the statistical value from 97 to 200 eV photon
energy. For Kr at 10 eV kinetic energy, Huang et al (1981) calculated
the $3d_{5/2}:3d_{3/2}$ ratio to be 1.51, slowly decreasing from higher energy.
For Xe the calculated branching ratio has larger changes with energy.
At 9 eV kinetic energy, Huang et al (1981) predict $4d_{5/2}:4d_{3/2}$ to be
1.5, increasing from higher energy. For all three atoms, the threshold
shake-off fractions in Ar and Kr are the same for pairs of spin-orbit
split resonances, e.g. Kr $3d_{5/2}$ → 5p and $3d_{3/2}$ → 5p.

The resonant threshold intensities increase from Ar to Kr to Xe.
In part, this trend results from the narrowing of the shake-off kinetic-
energy distribution in going from Ar to Xe. Considering the first

resonances of the three atoms, the maximum kinetic energy for two emitted electrons decreases from 201.0 eV (Ar) to 52.6 eV (Kr) and to 32.0 eV (Xe) (Moore 1949, 1952, Dutil and Marmet 1980). In the case of double Auger above threshold, the increasing trend of threshold intensities may be compared with the results of ion measurements. Above the inner-shell threshold but below the threshold for double ionization of an inner and outer electron, the double Auger probability can be inferred from the triple ion / double ion ratio R: $R[Ar(L_{2,3}-MMM)] =$ 0.11, $R[Kr(M_{4,5}-NNN)] = 0.17$, and $R[Xe(N_{4,5}-OOO)] = 0.19$ (Hayaishi et al 1984). The increasing double Auger probability with Z correlates with the decreasing binding energy and increasing <r> of a valence electron.

---

4. Threshold electron lineshapes, post-collision interaction (PCI)

Using a semi-classical model, Niehaus (1977) calculated an Auger lineshape which depends on the lifetime of the hole state τ and the excess photon energy above threshold $\Delta = h\nu - IP$. Since the Auger energy gain equals the photoelecton energy loss, his expression may be converted into a lineshape for the threshold photoelectron. Starting from his Eqs. (6), (7), and (14), and setting the Auger energy shift equal to Δ because 0 eV kinetic energy electrons are detected, we have:

$$P(\Delta) = \frac{1}{2\tau \, \Delta^{5/2}} \exp(-t_* / \tau) \tag{4}$$

where $t_* = \frac{1}{\sqrt{2} \, \Delta} \frac{\sqrt{2}}{\sqrt{\Delta}} - \sqrt{1+\Delta} - \frac{1}{2\sqrt{\Delta}} (1.763 + \ln[\frac{\sqrt{1+\Delta} - \sqrt{\Delta}}{\sqrt{1+\Delta} + \sqrt{\Delta}}])\}.$ (5)

The peaks at the inner-shell thresholds were fit to the Niehaus function convoluted with a gaussian representing the monochromator bandwidth.

These fits are depicted in Fig. 1 (Ar $2p_{3/2}$, $2p_{1/2}$), Fig. 2 (Kr $3d_{5/2}$, $3d_{3/2}$), and Fig. 3 (Xe $4d_{5/2}$, $4d_{3/2}$). For all three threshold scans the agreement between the fit and the data is excellent, confirming the validity of the Niehaus model, even when the Auger decay occurs while the photoelectron is still near the nucleus. In principle, interference could be present in the second threshold peak since paths through the two $j=1\pm1/2$ hole states can reach the same multiple-ion final states. This interference is not observed, perhaps because the threshold intensity sums over a number of Auger transitions, or perhaps because of insufficient resolution.

Table 2 displays the natural linewidths of the resonances Ar $2p_{3/2}$ → 4s from King et al (1977, 1985) and Kr $3d_{5/2}$ → 5p and Xe $4d_{5/2}$ → 6p from fits of our resonant threshold intensities using a Voigt function. These values for the Kr and Xe resonant linewidth agree reasonably well with those of King et al and Hayaishi et al (1984). The observation of Hayaishi et al that the linewidths for Kr and Xe are the same for all np resonances is consistent with the present results. Along with the resonance linewidths, Table 2 also shows the widths $1/\tau$ of the Neihaus function (Neihaus 1977) which best fit the threshold photoelectron peak shapes, from the PCI theory fits. For Ar and Kr, the linewidths (and lifetimes) of the resonance and threshold peaks agree within error, which is expected since the primary Auger process will be little perturbed by the presence of a bound Rydberg electron or slow photoelectron. For Xe, however, the threshold linewidth is significantly smaller than the resonant linewidth. The apparent longer lifetime of the Xe 4d hole at threshold may result from Neihaus's

neglect (Neihaus 1977) of the time interval taken for the Auger electron to overtake the photoelectron. In Xe this transit time will be longer than in Ar and Kr, since the average Auger energy is smaller. No comparison has been made to the calculated PCI lineshape of Russek and Mehlhorn (1986), whose expression contains terms which diverge for 0 eV photoelectron energy. From the comparison of the kinetic energy of the Xe $N_5O_{23}O_{23}$ $^1S_0$ with the predictions of Russek and Mehlhorn, Borst and Schmidt (1986) inferred a natural linewidth of 0.11 eV. An alternative explanation of the Xe threshold width is that the interaction between a slow photoelectron and a slow Auger electron cannot be approximated simply by a change in the photoelectron potential from $1/r$ to $2/r$.

5. Resonant kinetic energy spectra

To view the total picture of a resonance decaying into shake-off, Auger-like and main-line channels, electron spectra containing electrons of all kinetic energies must be measured because only for Xe are such spectra available in the literature (Becker et al 1984). Figures 5-7 show spectra taken at the $2p_{3/2} \rightarrow 4s$ resonance of Ar, the $3d_{5/2} \rightarrow 5p$ resonance of Kr and the $4d_{5/2} \rightarrow 6p$ resonance of Xe. By the subtraction of a near-lying off-resonance spectrum, the ns^{-1} and np^{-1} main lines and $np^4n'l$ satellites have been eliminated in each case. However, as has been discussed above, autoionization into main-line channels is weak (Southworth et al 1983, Hayaishi et al 1984, Becker et al 1986, Lindle et al 1986).

These spectra have three types of features. Discrete peaks observed at higher kinetic energies result from Auger-like transitions

in which the excited electron plays a spectator role or is shaken up into a higher nl orbital The final states corresponding to some of the peaks at higher energy can decay further. At lower kinetic energies, discrete peaks are caused by second step Auger transitions from these excited states of the singly charged ion. Table 3 shows the energies and assignments of some of the second-step decays. This list of second-step Auger peaks is incomplete, and does not reflect completely the large possible number of these transitions. Lastly, a continuous background is observed resulting from shake-off transitions. In agreement with the results of the threshold scans, the continuous electron signal is strong in the photoelectron spectra. It should also be noted for Kr and Xe that the continuous background at high kinetic energy is low, even though the shake-off distribution resulting in np^{-2} final states should extend to 52.5 eV for Kr and 32.0 eV for Xe (Moore 1952, Dutil and Marmet 1980). This observation suggests that np^{-2} is not an important final configuration for shake-off.

The resonant shake-off intensities given in Table 3 were evaluated by drawing a linear background function underneath the peaks in Figs. 5-7. A number of unresolved peaks, taken together, could resemble background. This is a concern which is reflected in the large error bars. In the analysis of the Kr and Xe spectra, we used the higher-resolution spectra of Aksela et al (1986a, b) as a guide for the number and location of the peaks. To obtain the shake-off probability, the total number of background electrons must then be divided by the average number of electrons ejected in a single shake-off transition, approximately $(2\sigma_{2+} + 3\sigma_{3+}) / (\sigma_{2+} + \sigma_{3+})$. The ion ratios (Hayaishi et al

1984) measured on these resonances give 2.1 shake-off electrons per event for Ar, 2.1 for Kr, and 2.0 for Xe. The fractions of these resonances resulting in shake-off and second-step Auger transitions are displayed in Table 3. The reported second-step fractions must be viewed as lower bounds, partly because they only include peaks at energies above 5 eV and partly because of the uncertainty in the shake-off background subtraction. In Kr, for example, by assuming that $4s^{-1}4p^{-1}nl$ and $4s^{-2}nl$ states lead to further Auger electrons, while $4p^{-2}nl$ states do not, an alternative estimate of the second-step Auger contribution can be obtained. In the case of Kr, this method gave a much higher value for the 2nd step Auger, 45 % of the resonant strength. The resulting shake-off fraction is still within the error limits of 37(8) %.

The shake-off contributions increase from Ar to Kr to Xe. The shake-off fraction for the Xe $4d_{5/2} \to 6p$ resonance agrees well with the result of Becker et al (1984), 44 %. For all three atoms, the resonant shake-off intensity is of comparable or greater strength than the two-step Auger-like transitions. This result conflicts with the discussions of Hayaishi et al (1984) and Eland et al (1986), who tentatively concluded that Ar^{2+}, Kr^{2+}, and Xe^{2+} dominantly result from sequential decays. With regard to the formation of triply charged ions, three discrete steps are excluded by energy considerations. Therefore, triply charged ions should always result from shake-off either directly from the neutral excited state or possibly in two steps, such as Kr $3d^{-1}np \to$ $Kr^+ 4s^{-2}np \to Kr^{3+}4p^{-2}$. In Xe, the $4d_{5/2} \to 6p$ resonance is only 0.7 eV above the Xe^{3+} threshold (Dutil and Marmet 1980), and can only access

Xe^{3+} when three electrons leave simultaneously with very low kinetic energy. Qualitative ion ratios can be derived from the analysis of these photoelectron spectra. The derived ion ratios agree with the mass spectrometry results for Ar and Xe (Hayaishi et al 1984, Eland et al 1986), but not for Kr, for which a very small cross section to Kr^+ was reported by Hayaishi et al (1984). Compared with a total σ of 7.5 Mb at the Kr $3d_{5/2} \rightarrow 5p$ resonance (Hayaishi et al 1984), Kr^+ will be formed from the $4s^{-1}$ and $4p^{-1}$ main lines, 0.50 Mb (Lindle et al 1986), and from nearly all the $4p^{-2}nl$ spectator lines, 1.5 Mb. (The Kr^+ $(^1S)4p^{-2}6p$ state can further Auger decay). It is interesting that Hayaishi et al (1984) observed no PCI effect in the Kr and Xe ion yields. Related to the high shake-off probability, the slow photoelectron cannot be captured in a high Rydberg state.

Figure 8 shows the low-kinetic-energy distribution of emitted electrons on two resonances of Kr. The intensity decreases steeply from 0 eV kinetic energy for both resonances. For the $3d_{5/2} \rightarrow 5p$ resonance, as seen in Fig. 6, a number of discrete transitions fall between 5 and 10 eV. The kinetic-energy distribution of resonant shake-off electrons should resemble that of the nonresonant double photoionization of valence shells, e.g. $Ne + h\nu \rightarrow Ne^{2+} 2p^4 + 2e^-$, which has been studied experimentally by Carlson (1967) and theoretically by Chang and Poe (1975). For Ne with the ejected electrons sharing a total kinetic energy (TKE) of ~200 eV, Carlson observed an order-of-magnitude decrease from TKE to TKE/2. An identical decrease must occur between 0 and TKE/2. Using many-body perturbation theory, Chang and Poe calculated kinetic-energy distributions, also for Ne, which become less peaked as

the photon energy decreases toward the double-ionization threshold.
Resonant shake-off transitions to double ions reach the same final
states as valence double photoionization, and the two processes may be
considered to be the same.

For the Kr $3d_{5/2} \rightarrow 7p$ resonance the intensity decreases from 0 eV
more quickly than for the 5p resonance. A similar change in slope was
observed for the Xe $4d_{5/2} \rightarrow 6p$ and 7p low-kinetic-energy distributions.
In general, the shake-off distributions of higher nl resonances seem to
be more sharply peaked at 0 eV. Theoretical effort aimed at explaining
this unexpected behavior of the resonant shake-off intensity would be
valuable. As a consequence of the changing kinetic-energy
distributions, the threshold intensities of the resonances cannot be
interpreted as proportional to the total shake-off probability. In
part, the higher fractional threshold intensity of the Kr $3d_{5/2} \rightarrow 7p$
resonance must result from the sharper peaking of the shake-off
distribution at 0 eV. Although photoelectron spectra were taken on some
of the higher nl resonances, their quality was insufficient to confirm
that the total shake-off contribution increases with n as implied by the
ion yields.

From the photoelectron spectra and low-kinetic-energy
distributions, a number of observations can be made about the shake-off
decay of these resonantly excited states. First, shake-off is a strong
decay channel which is inconsistent with the spectator model as a
complete description of resonant decay. Its importance is less
surprising when compared with the intensity of double-Auger transitions
above threshold. Shake-off makes a major contribution to the double-ion

yield and is solely responsible for the triply-charged ions. For the first resonances the importance of shake-off increases from Ar to Kr and reaches a probability of about 50 % for Xe. The main final states of shake-off are configurations other than np^{-2}, suggesting the influence of configuration interaction in the decay final states. The resonant shake-off distribution has a maximum at zero kinetic energy. From 0 eV, the slope of the decreasing intensity becomes steeper for the higher n resonances.

6. Shake calculation

Carlson et al (1966, 1973) used shake theory and single-configuration wavefunctions to calculate shake-off probabilities accompanying photoionization or Auger decay. The mechanism considered by this model is the sudden change of the potential The shake probability P_{nl}, which includes shake-up to discrete levels as well as shake-off to the continuum, is given by:

$$P_{nl} = 1 - [\int \Psi_{nl}(A_f)\Psi_{nl}(A_i)dr]^{2N} - P_F. \qquad (1)$$

Here, Ψ_{nl} represent the neutral (A_i) and ionic (A_f) radial wavefunctions (multiplied by r), and N is the number of electrons occupying the nl subshell. P_F corrects for the finite calculated probabilities for transitions to filled subshells. In the cases discussed below, P_F is not important. The agreement with experiment is qualitatively good, within a factor of two, except when photoionization (or Auger decay) and shake-off involve two electrons from the same shell. In this case, many-body effects cannot be neglected. As a result, the shake-theory

estimates for double Auger, for example Ar $L_{2,3}$-MMM, are much too low (Carlson and Krause 1966).

Table 4 shows the results of a calculation using Eq. (1) for the shake probability on the Ar 2p → ns, nd, Kr 3d → np and Xe 4d → np resonances. The calculations were performed with the Robert Cowan RCN program (Cowan 1981). We consider for each atom the transition in which a valence p electron fills the hole and another valence p electron is ejected. Figure 9 shows the radial wavefunctions of Ar before and after the Auger-like decay: Ar $2p^{-1}3d$ → Ar^{+} $3p^{-2}3d$. The electron kinetic energy will be somewhat higher than the Ar LMM Auger energy above threshold, about 200 eV, and as a result the sudden approximation should be valid. For Kr and Xe the Auger kinetic energies are less, from below 10 eV to 60 eV (Aksela et al 1986a, b), and the sudden approximation may not be valid.

The calculated shake probability of the valence electrons is quite small, i.e. < 1 %. This result does not have predictive value since all the electrons involved are from the M shell and correlation cannot be neglected. It is interesting, however, that for valence orbitals the potential change resulting from the Auger-like transition is small: an extra core electron is gained which screens the outer electrons well, while two valence electrons, which screen imperfectly, are lost. These effects largely cancel. The 3s and 3p radial wavefunctions of Ar^{+} are in fact nearly indistinguishable from those of Ar shown in Fig. 9.

The calculated shake probability of the Rydberg electron is large, and it increases with n until it reaches nearly unity at the third or fourth resonanace. The behavior of all three atoms is rather similar.

Qualitatively these results may be explained by considering the slowly-varying, nearly-Coulombic potential at large r, approximately given by $\frac{1}{r}$ or $\frac{2}{r}$, which when changed from $\frac{1}{r}$ to $\frac{2}{r}$ may cause the Rydberg orbital to move dramatically toward the nucleus, as seen for Ar 3d in Fig. 1. At smaller r there exists a potential barrier from the centrifugal and Coulomb repulsion terms. For higher n the Rydberg orbital, being further from the repulsive barrier, can contract more upon ionization. The potential at large r should be similar for all three atoms, in agreement with the similar shake probabilities. In addition, there is a dependence on l, with the shake probability following the sequence $P_d > P_p > P_s$.

Further caution must be exercised with regard to the results of the shake calculation. If overlap integrals are calculated between the Rydberg orbital before Auger-like decay and higher Rydberg orbitals afterwards, the excitation to discrete levels, for example Xe $4d^{-1}6p \to$ Xe$^+$ $5p^4 7p$, can be estimated. However, the resulting excitation probability accounts for nearly the total shake probability, which does not agree with the experimental observation of the importance of shake-off. It is therefore concluded that the accuracy of this calculation is not sufficient to partition the total shake contribution into shake-up and shake-off components. The shake calculation does give the correct qualitative results that the Rydberg electron has a high shake-off probability, and that it increases with n.

7. Conclusion

From the measurement of electron spectra at zero and higher kinetic energies, a detailed, though qualitative picture of shake-off has emerged for the resonances below the Ar 2p, Kr 3d, and Xe 4d thresholds. First of all, shake-off together with shake-up is a very important channel in the decay of the hole. This result restricts the applicability of the spectator model. For the first resonances, Ar $2p_{3/2} \rightarrow 4s$, Kr $3d_{5/2} \rightarrow 5p$, and Xe $4d_{5/2} \rightarrow 6p$, the shake-off probability increases from Ar to Kr and becomes about 50 % for Xe. The shake-off intensity also increases with the quantum number n of the Rydberg electron; i.e., with the Rydberg orbital becoming more diffuse. In resonant shake-off, a valence electron and the Rydberg electron are usually ejected. For the Kr $3d_{5/2} \rightarrow 5p$ and Xe $4d_{5/2} \rightarrow 6p$ resonances, it was found that np^{-2} final states are unimportant. This observation suggests the influence of final-ionic-state configuration interaction. The kinetic energy distribution of shake-off electrons decreases from 0 eV, with a steeper slope for higher-n resonances. The high probability for ejection of the Rydberg electron is explained by the independent-electron shake calculation. When the core rearranges to fill the hole, the potential for the nl Rydberg orbital becomes more attractive, which causes that orbital to contract and makes it likely that the Rydberg electron will go into another orbital Further study of shake-off on these and other resonances is needed. Higher resolution photoelectron spectra could more quantitatively determine the shake-off contribution by clearly distinguishing between the many peaks from second-step transitions and the background. A more sophisticated calculation of the

resonant shake-off probability, including electron correlation effects, would be valuable.

References

Aksela H, Aksela S, Bancroft G M, Tan K H and Pulkkinen H 1986a Phys. Rev. A 33 3867-75

Aksela H, Aksela S, Pulkkinen H, Bancroft G M and Tan K H 1986b Phys. Rev. A 33 3876-84

Aksela S, Tan K H, Bancroft G M, Aksela H, Yates B W and Coatsworth L L 1985 Phys. Rev. A 32 1219-21

Baer T, Guyon P M, Nenner I, Tabche-Fouhaille A, Botter R, Ferreira L F A and Govers T R 1979 J. Chem. Phys. 70 1585-92

Becker U, Hölzel R, Kerkhoff H G, Langer B, Szostak D and Wehlitz R 1984 BESSY Annual Report 121-3

Becker U, Prescher T, Schmidt E, Sonntag B and Wetzel H E 1986 Phys. Rev. A 33 3891-9

Borst M and Schmidt V 1986 Phys. Rev. A 33 4456-8

Carlson T A 1967 Phys. Rev. 156 142-9

Carlson T A and Krause M O 1966 Phys. Rev. Lett. 17 1079-83

Carlson T A, Krause M O, Grimm F A, Keller P R and Taylor J W 1982 Chem. Phys. Lett. 87 552-5

Carlson T A and Nestor C W 1973 Phys. Rev. A 8 2887-94

Chang T N and Poe R T 1975 Phys. Rev. A 12 1432-9

Codling K and Madden R P 1964 Phys. Rev. Lett. 12 106-8

Cowan R D 1981 The Theory of Atomic Structure and Spectra (Berkeley: Univ. of California Press)

Dutil R and Marmet P 1980 Int. J. Mass Spect. Ion Phys. 35 371-9

Eland J H D, Wort F S, Lablanquie P and Nenner I 1986 Zeitschrift für Physik to be published.

Fano U and Cooper J W 1965 Phys. Rev. 137 A1364-79

----1968 Rev. Mod. Phys. 40 441-507

Hayaishi T, Morioka Y, Kageyama Y, Watanabe M, Suzuki I H, Mikuni A,

Isoyama G, Asaoka S and Nakamura M 1984 J. Phys. B: At. Mol. Phys.

17 3511-27

Heimann P A, Becker U, Kerkhoff H G, Langer B, Szostak D, Wehlitz R,

Lindle D W, Ferrett T A and Shirley D A 1986 Phys. Rev. A 34 3782-91

Huang K N, Johnson W R and Cheng K T 1981 At. Data Nucl. Data Tables 26

33-45

Kennedy D J and Manson S T 1972 Phys. Rev. A 5 227-47

King G C, Tronc M, Read F H and Bradford R C 1977 J. Phys. B: At. Mol.

Phys. 10 2479-94

King G C and Read F H 1985 Atomic Inner-shell Physics ed B Crasemann

(New York: Plenum)

Lindle D W, Heimann P A, Ferrett T A, Piancastelli M N and Shirley D A

1986 to be published.

Moore C E 1949 Atomic Energy Levels NBS Circular No 467, vol 1

(Washington, DC: US Govt Printing Office)

----1952 Atomic Energy Levels NBS Circular No 467, vol 2 (Washington,

DC: US Govt Printing Office)

Niehaus A 1977 J. Phys. B 10 1845-57

Russek A and Mehlhorn W 1986 J. Phys. B: At. Mol. Phys. 19 911-27

Schmidt V, Krummacher S, Wuilleumier F and Dhez P 1981 Phys. Rev. A 24

1803-11

Southworth S H, Becker U, Truesdale C M, Kobrin P H, Lindle D W, Owaki S

and Shirley D A 1983 Phys. Rev. A 28 261-79

Walker T E H and Waber J T 1974 J. Phys. B: At. Mol. Phys. 7 674-92

White M G, Rosenberg R A, Gabor G, Poliakoff E D, Thorton G, Southworth

S H and Shirley D A 1979 Rev. Sci. Instrum. 50 1268-73

Wight G R and Van der Wiel M J 1977 J. Phys. B: At. Mol. Phys. 10 601-10

Wiley W C and McLaren I H 1955 Rev. Sci. Instrum. 26 1150-7

Yates B W, Tan K H, Coatsworth L L and Bancroft G M 1985 Phys. Rev. A 31

1529-34

Table 1. Threshold intensities from this work, and energies and oscillator strengths from King et al (1977, 1985)

Atom	Transition	Energy (eV)	Oscillator Strength f	Threshold Intensity I_{th}	$\frac{1}{f}\left.\frac{df_s}{dKE}\right|_0 (eV^{-1})$
Ar	$2p_{3/2} \rightarrow$ 4s	244.39(1)	0.51(5)	0.22(5)	0.015(4)
	3d	246.93(1)	1	1.00(15)	0.034(6)
	4d	247.67(1)	0.63(4)	6.5(6)	0.22(3)
	5d	248.03(2)	0.39(4)		
	ϵs,d	248.63(1)	1.38(8)	40.3(10)	
	$2p_{1/2} \rightarrow$ 4s	246.51(1)	0.28(5)	0.19(10)	0.023(13)
	3d	249.07(1)	0.50(3)		
	4d	249.82(1)	0.30(3)	2.7(7)	0.20(5)
	5d	250.17(2)	0.14(3)		
	ϵs,d	250.78(1)	0.82(6)	24.7(4)	

Table 1. continued.

Atom	Transition		Energy (eV)	Oscillator Strength f	Threshold Intensity I_{th}	$\frac{1}{f}\frac{df_s}{dKE}\Big|_0 (eV^{-1})$
Kr	$3d_{5/2}$ →	5p	91.20(1)	1.0	1.00(4)	0.14(2)
		6p	92.56(1)	0.37(1)	0.57(3)	0.21(3)
		7p	93.06(1)	0.12(1)	0.29(1)	0.33(6)
		8p	93.30(3)	0.08(4)	0.24(1)	0.41(22)
		εp	93.79(2)	0.36(8)	2.57(12)	
	$3d_{3/2}$ →	5p	92.43(1)	0.63(1)	0.66(3)	0.15(2)
		6p	93.81(1)	0.23(1)	0.41(3)	0.25(4)
		7p	94.32(2)	0.087(10)	0.18(2)	0.29(7)
		8p	94.57(3)	0.034(14)	0.14(2)	0.57(30)
		εp	95.04(3)	0.22(4)	1.62(8)	
Xe	$4d_{5/2}$ →	6p	65.11(1)	1.0	1.00(4)	0.29(5)
		7p	66.38(1)	0.334(6)	0.55(3)	0.47(9)
		8p	66.85(1)	0.112(7)	0.21(1)	0.53(10)
		εp	67.55(1)	0.37(6)	1.60(8)	
	$4d_{3/2}$ →	6p	67.04(1)	0.74(2)	0.69(5)	0.27(4)
		7p	68.35(1)	0.226(7)	0.34(2)	0.43(6)
		8p	68.84(2)	0.092(12)	0.14(1)	0.42(9)
		εp	69.54(1)	0.29(2)	0.87(4)	

Table 2. Natural linewidth of the inner-shell resonance of lowest photon

energy for Ar, Kr, and Xe, and the width $(1/\tau)$ of the Niehaus

function (Eqns (4) and (5)) which best fits the threshold peaks.

Atom	Threshold Width Niehaus Function (eV)	Resonance Natural Linewidth (eV)		
		this work	King et al (1985)	Hayaishi et al (1984)
Ar	0.12(1)		0.116(3)	
Kr	0.08(1)	0.088(6)	0.083(4)	0.108
Xe	0.07(1)	0.102(5)	0.111(4)	0.105

Table 3. The contribution of shake-off and second-step Auger transitions in the total decay of the first resonances in Ar, Kr, and Xe.[a]

Resonance	Shake-off Fraction	2nd Step Auger Fraction	Energy (eV)	Identification
Ar $2p_{3/2} \rightarrow 4s$	16(8) %	18 %	7.0(7)	
			15.1(4)	
Kr $3d_{5/2} \rightarrow 5p$	37(8) %	16 %	3.3(3)	
			6.1(3)	$4s^{-1}4p^{-1}(^1P)5p \rightarrow 4p^{-2}\ ^1S$ $4s^{-2}5p \rightarrow 4s^{-1}4p^{-1}\ ^1P$
			7.9(3)	$4s^{-1}4p^{-1}(^1P)5p \rightarrow 4p^{-2}\ ^1D$
			9.6(3)	$4s^{-2}5p \rightarrow 4s^{-1}4p^{-1}\ ^3P$ $4s^{-1}4p^{-1}(^1P)5p \rightarrow 4p^{-2}\ ^3P$
			13.8(3)	$4p^{3}4d5p \rightarrow 4p^{-2}\ ^1D$
Xe $4d_{5/2} \rightarrow 6p$	50(10) %	18 %	6.1(3)	$5s^{-1}5p^{-1}6p \rightarrow 5p^{-2}\ ^3P,^1D$ $5s^{-2}6p \rightarrow 5s^{-1}5p^{-1}\ ^3P$
			10.0(3)	$5p^{-3}5d6p \rightarrow 5p^{-2}\ ^1D$

[a]All fractions represent a percentage of the total σ on the resonance excluding the nonresonant valence σ_{sat}, σ_s and σ_p.

Table 4. The calculated shake probabilities P_{nl} accompanying Auger-like decay,[a] for example Ar $2p^{-1}4s \rightarrow Ar^{+} 3p^{-2}\epsilon s$.

Atom	orbital	P_{nl}	Atom	orbital	P_{nl}	Atom	orbital	P_{nl}
Ar	4s	0.13	Kr	5p	0.22	Xe	6p	0.21
	5s	0.49		6p	0.65		7p	0.63
	3d	0.78		7p	0.96		8p	0.95
	4d	0.99		8p	0.98		9p	0.98
	5d	0.89						

[a]For each resonance the probability of ejection (or excitation) of the Rydberg electron is shown.

Figure captions

Fig. 1 A threshold scan over the Ar $2p^{-1}ns$, nd resonances and 2p
thresholds. The curve reproduces a fit.

Fig. 2 A threshold scan over the Kr $3d^{-1}np$ resonances and 3d thresholds.
The curve reproduces a fit.

Fig. 3 A threshold scan over the Xe $4d^{-1}np$ resonances and 4d thresholds.
The curve reproduces a fit.

Fig. 4 An energy level diagram for the first Kr resonance. The arrows
show the excitation and three types of single step decay which
result in the ejection of two or more electrons.

Fig. 5 An electron difference spectrum of Ar taken at 244.4 eV photon
energy on the $2p_{3/2}^{-1}4s$ resonance and at 55° with respect to the
light polarization vector. Nonresonant contributions have been
removed by subtracting a spectrum taken at 242.2 eV photon energy.
The labels give only the most important final states.

Fig. 6 Electron difference spectrum, like Fig. 5, for Kr at 91.2 eV on the
$3d_{5/2}^{-1}5p$ resonance and at 0°. Non-resonant spectrum at 90.2 eV has
been subtracted.

Fig. 7 Electon difference spectrum, like Fig. 5, for Xe at 65.1 eV on the
$4d_{5/2}^{-1}6p$ resonance and at 0°. Non-resonant spectrum at 64.1 eV has
been subtracted. This difference spectrum has been corrected for
the consequences of extra electrons being in an adjacent "bucket"
in the storage ring.

Fig. 8 The low kinetic energy distribution of electrons ejected on two Kr
resonances: Kr $3d_{5/2}^{-1}5p$ and $3d_{5/2}^{-1}7p$.

Fig. 9 The outer radial wavefunctions ψ_{nl} of Ar calculated for the configuration $2p^{-1}3d$ and ψ_{3d} of Ar^+ $3p^{-2}3d$.
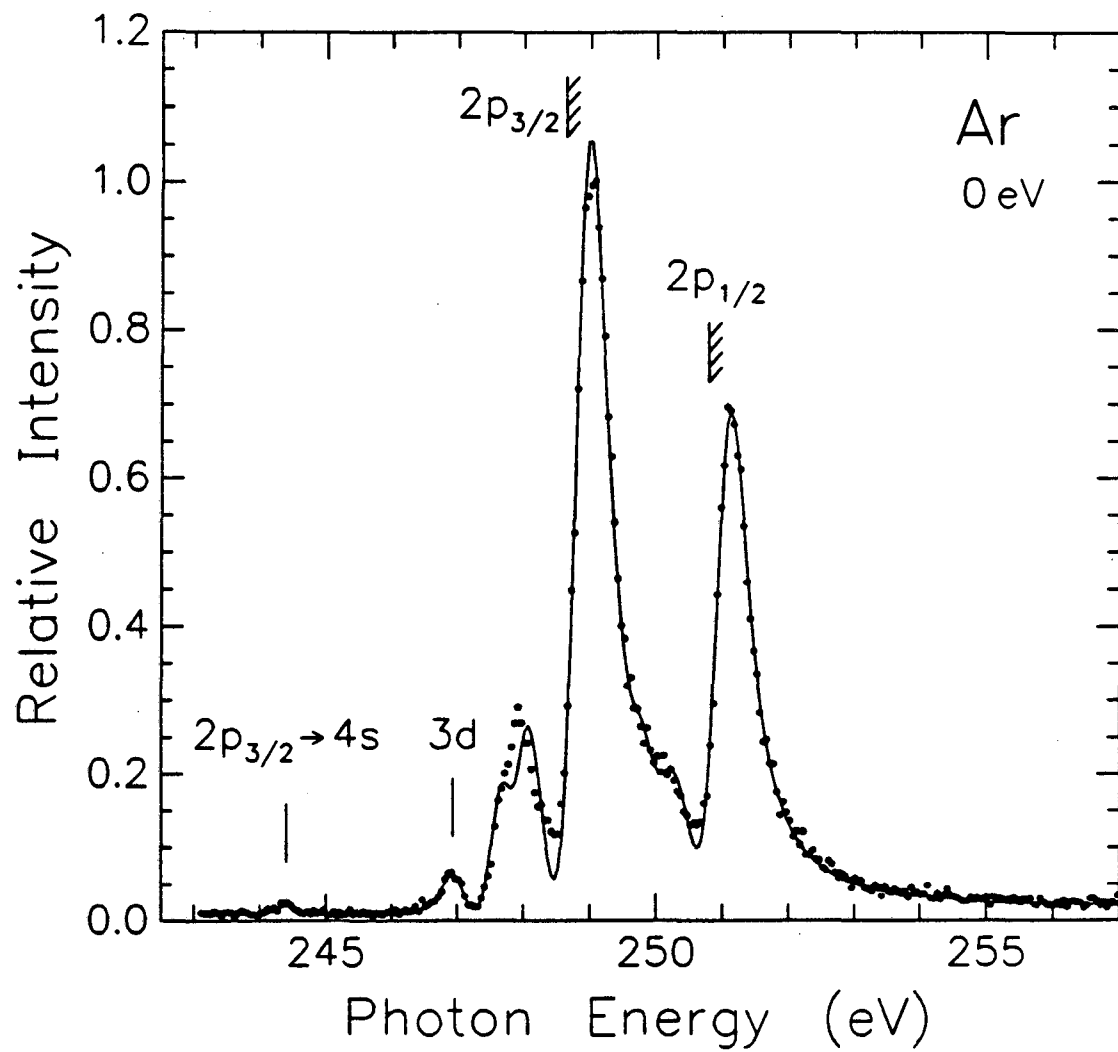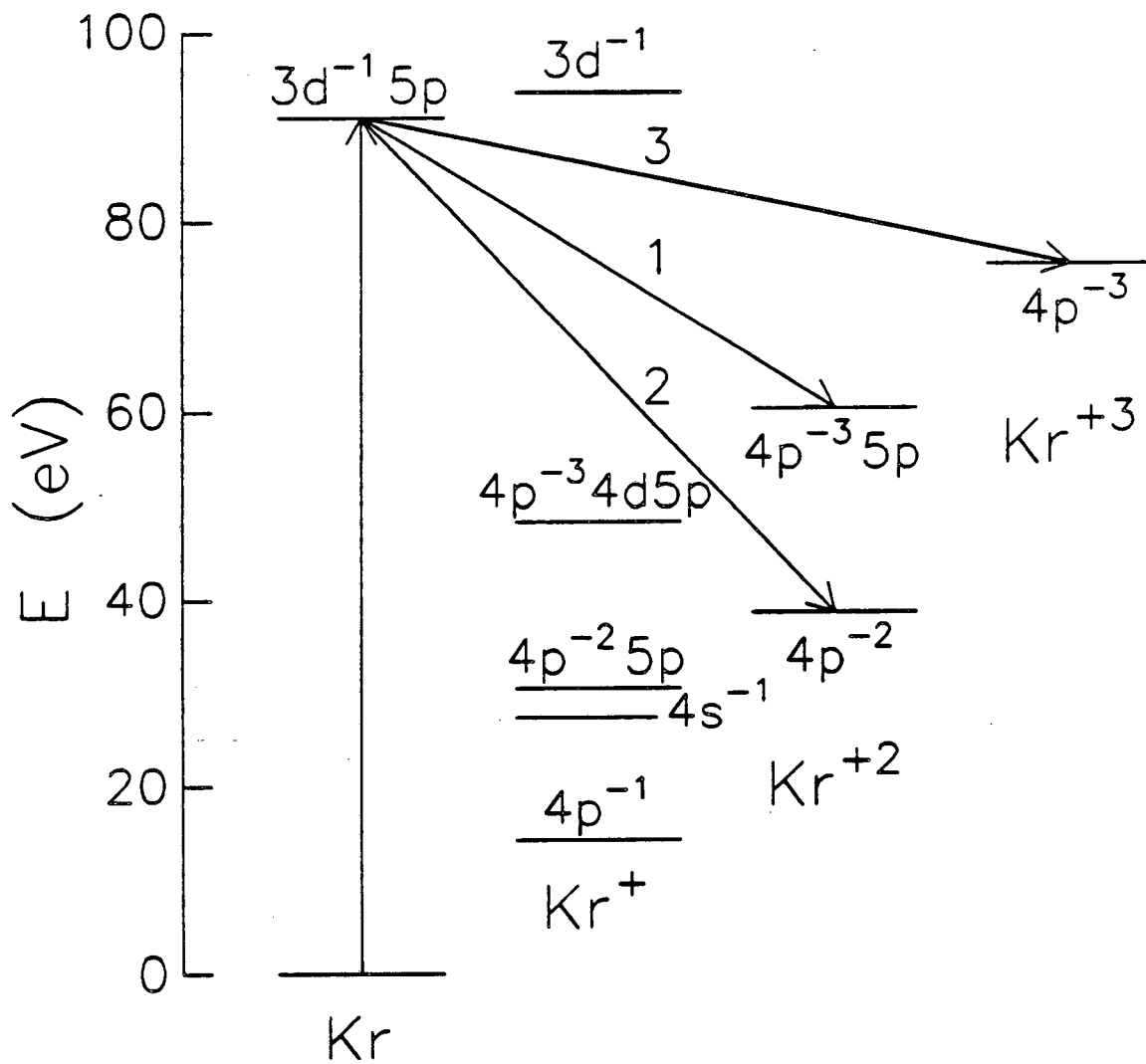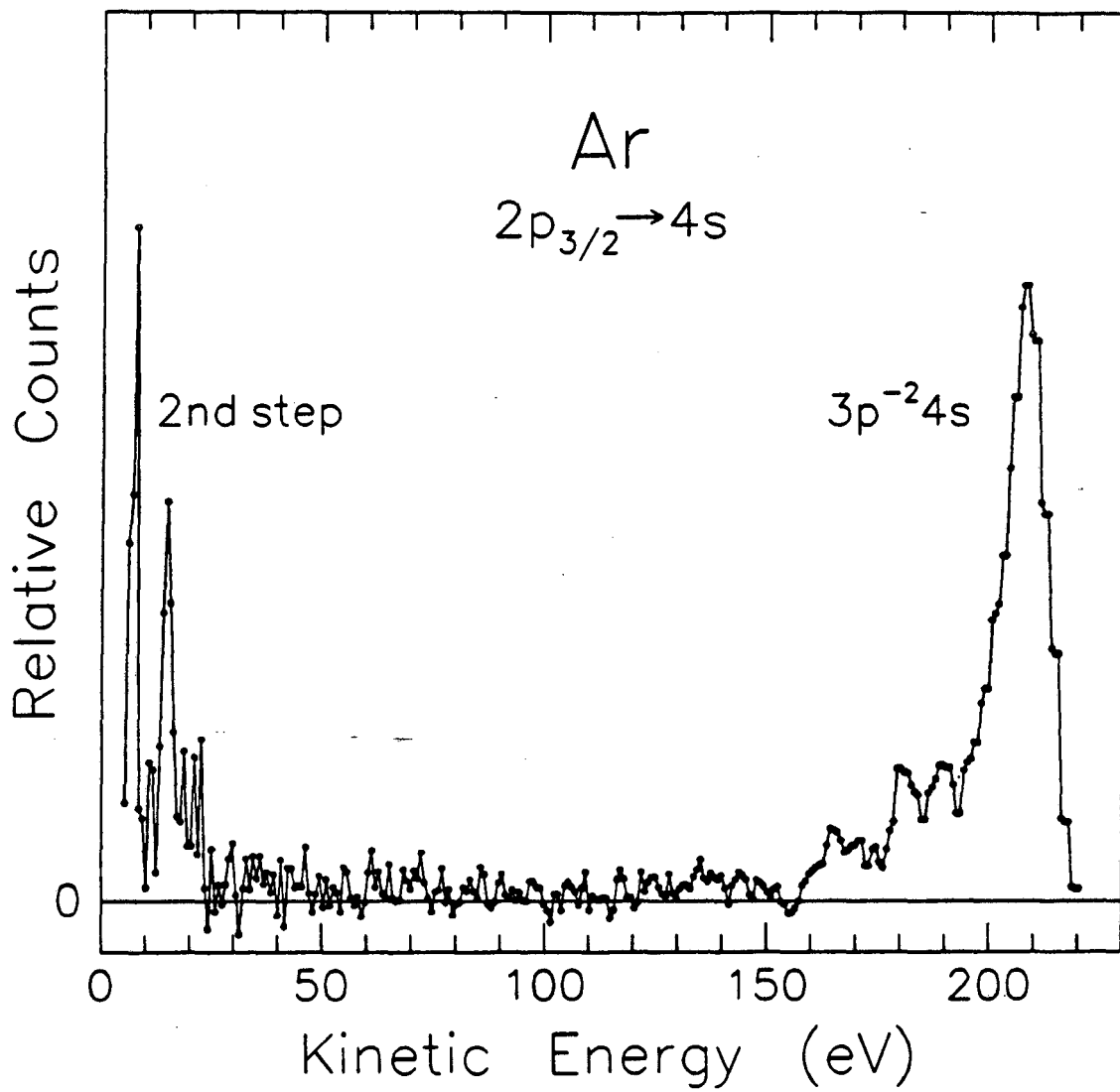
XBL 8611-4319

Figure 1
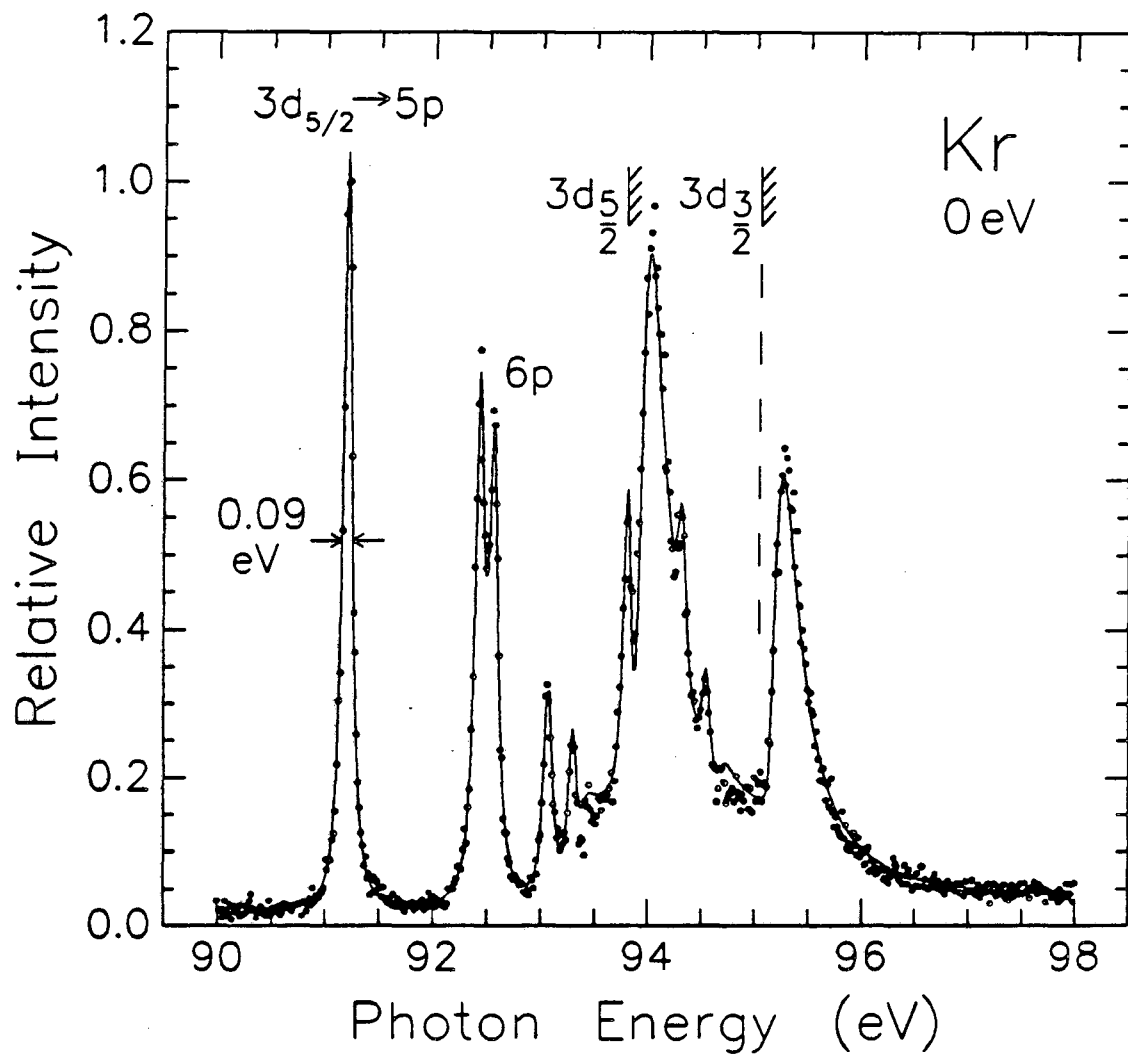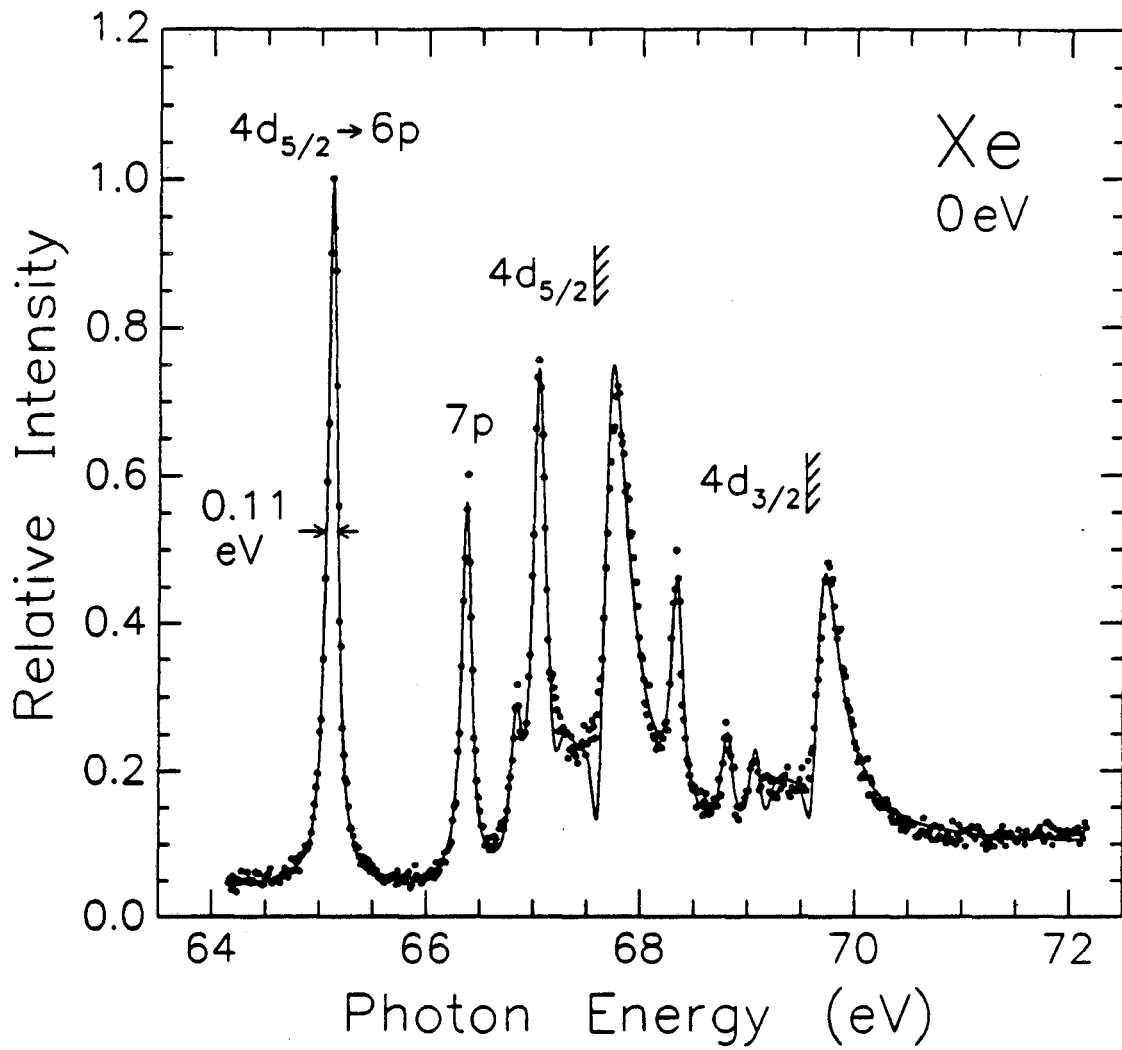
Figure 2

Figure 3

XBL 8611-4321

Figure 4

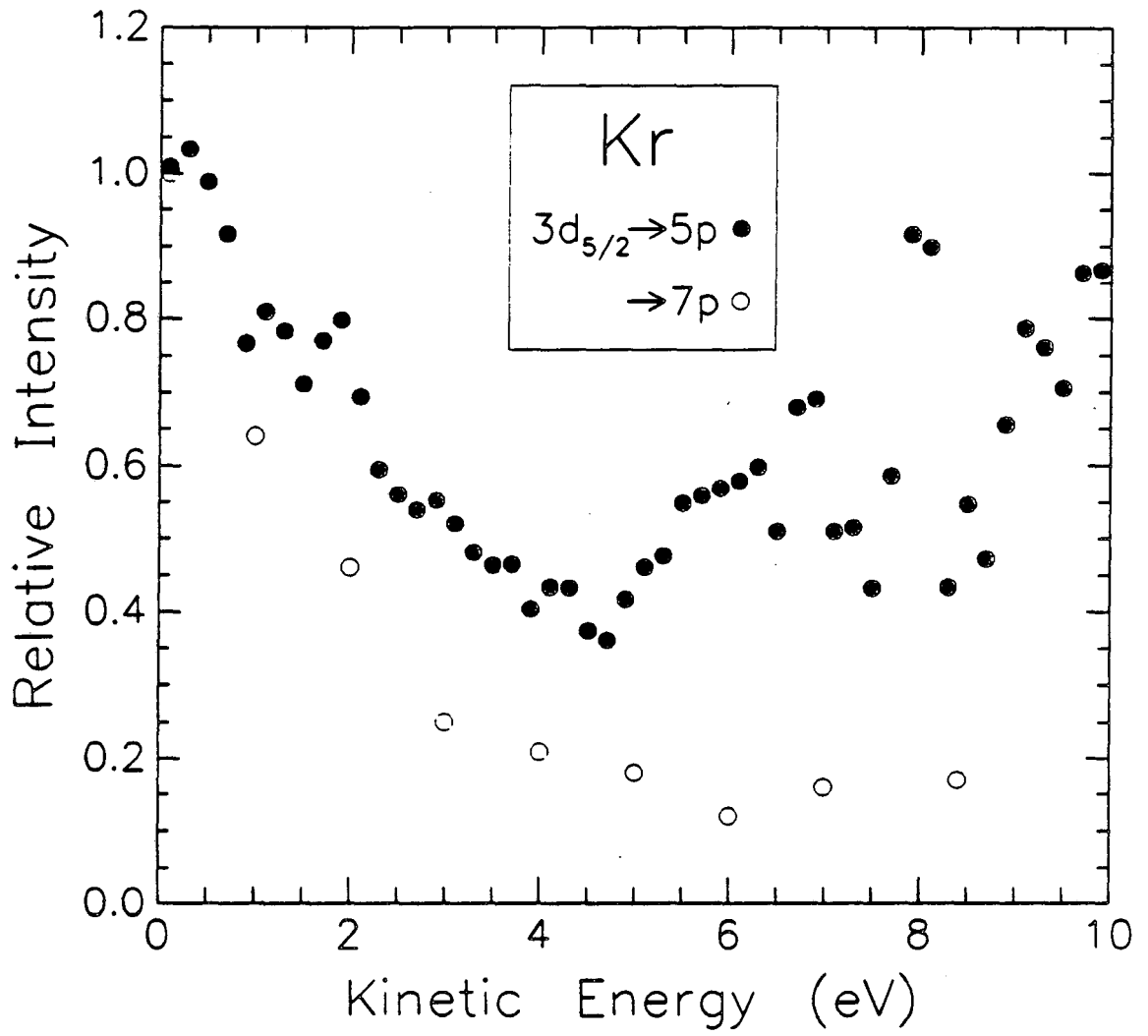XBL 8611-4318

XBL 8611-4322

Figure 5

Figure 6

Figure 7

Figure 8

XBL 8611-4325

XBL 8611-4326

Figure 9